

See discussions, stats, and author profiles for this publication at: <https://www.researchgate.net/publication/263207039>

Raman Imaging Providing Insights into Chemical Composition of Lipid Droplets of Different Size and Origin: In Hepatocytes and Endothelium

ARTICLE *in* ANALYTICAL CHEMISTRY · JUNE 2014

Impact Factor: 5.64 · DOI: 10.1021/ac501395g · Source: PubMed

CITATIONS

9

READS

96

6 AUTHORS, INCLUDING:



Katarzyna Majzner

Jagiellonian University

15 PUBLICATIONS 104 CITATIONS

[SEE PROFILE](#)



Neli Kachamakova-Trojanowska

Jagiellonian University

24 PUBLICATIONS 160 CITATIONS

[SEE PROFILE](#)



Stefan Chlopicki

202 PUBLICATIONS 1,928 CITATIONS

[SEE PROFILE](#)



Malgorzata Baranska

Jagiellonian University

159 PUBLICATIONS 1,868 CITATIONS

[SEE PROFILE](#)

Raman Imaging Providing Insights into Chemical Composition of Lipid Droplets of Different Size and Origin: In Hepatocytes and Endothelium

Katarzyna Majzner,^{†,‡} Kamila Kochan,^{†,‡} Neli Kachamakova-Trojanowska,[†] Edyta Maslak,[†] Stefan Chlopicki,^{†,§} and Małgorzata Baranska^{*,†,‡}

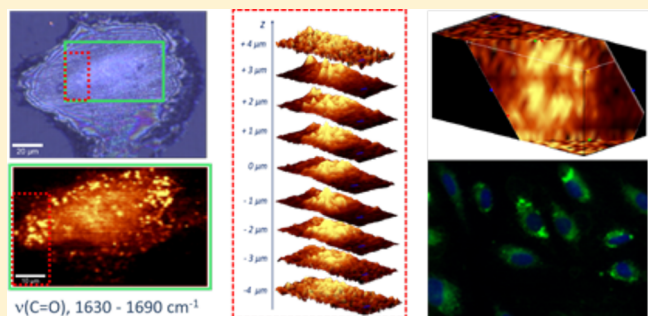
[†]Jagiellonian Centre for Experimental Therapeutics (JCET), Jagiellonian University, Bobrzański 14, Krakow, 30-348, Poland

[‡]Faculty of Chemistry, Jagiellonian University, Ingardena 3, Krakow, 30-060, Poland

[§]Department of Experimental Pharmacology, Chair of Pharmacology, Jagiellonian University, Grzegorzecka 16, Krakow, 31-531, Poland

Supporting Information

ABSTRACT: In this work, 3D linear Raman spectroscopy was used to study lipid droplets (LDs) *ex vivo* in liver tissue and also *in vitro* in a single endothelial cell. Spectroscopic measurements combined with fluorescence microscopy and/or histochemical staining gave complex chemical information about LD composition and enabled detailed investigations of the changes occurring in various pathological states. Lipid analysis in fatty liver tissue was performed using a dietary mouse model of liver steatosis, induced by a high fat diet (HFD). HFD is characterized by a high percentage of calories from saturated fat (60%) and reflects closely the detrimental effects of dietary habits responsible for increased morbidity due to obesity and its complications in well-developed Western societies. Such diets lead to obesity, hyperlipidemia, insulin resistance, and steatosis that may also be linked to endothelial dysfunction. In the present work, Raman spectroscopy was applied to characterize chemical composition of lipid droplets in hepatocytes from mice fed HFD and in the endothelium treated with exogenous unsaturated free fatty acid (arachidonic acid). The results demonstrate the usefulness of Raman spectroscopy to characterize intracellular lipid distribution in 2D and 3D images and can be used to determine the degree of saturation. Raman spectroscopy shows the potential to be a valuable tool for studying the role of LDs in physiology and pathology. The method is generally applicable for the determination of LDs of different size, origin, and composition. Moreover, for the first time, the process of LD formation in the endothelium was detected and visualized in 3D.



Lipid droplets (LDs) have been described in diverse cell types in histological and morphological studies for more than a 150 years. It is likely that structures referred to as “lipid bodies”, “lipid globules”, “lipid particles”, and “oil bodies” all represent lipid droplets. In most cell types, lipid droplets are usually less than 1 μm in size, although in hepatic steatosis, lipid droplets may reach 10 μm^1 .

At present, lipid droplets are under intensive study due to the increasing recognition of their significant role in many aspects of health and disease. Their function in the field of cell biology, the prevalence in metabolic syndromes, obesity, steatosis, and atherosclerosis have prompted medical research on LDs.^{2–6} Since many of these diseases manifest themselves by a considerable increase in lipid accumulation (e.g., in liver or arteries), leading to the formation of large lipid droplets far exceeding the size of individual cells, it is necessary to extend the study of lipid droplets to the tissue level.

LDs can also be found in many cell types including hepatocytes and endothelial cells (ECs) as lipid-rich, spherical

cytoplasmic inclusions with a distinctive architecture. In contrast to membranous organelles and cytoplasmic vesicles that have an aqueous content surrounded by a phospholipid bilayer membrane, LDs are composed of a neutral lipid core enclosed by a monolayer of phospholipids with associated proteins.^{2,7}

LDs were previously thought to be just an energy reservoir of the cell, but in recent years, it has become clear that they might have other functions.^{2,3,8–10} LDs are common in organelles of eukaryotic cells, but their biogenesis is not fully understood.^{11–13} It is accepted that LDs originate from the endoplasmic reticulum (ER), where neutral lipids are synthesized, and then, they aggregate within the hydrophobic core of the ER membrane. Upon reaching a critical size, LDs are thought to bud from the ER to form an independent

Received: April 16, 2014

Accepted: June 3, 2014

organelle, surrounded by a membrane monolayer. Even though this is a frequently postulated model for LDs biogenesis, alternative mechanisms have also been proposed.^{2,4–6,12,14}

The aim of this study was to investigate lipid droplets at different levels of biological sample complexity and, moreover, to show the utility of linear Raman imaging spectroscopy to monitor LDs of different size and origin focusing on their formation and chemical composition in hepatocytes *in situ* and in the cultured endothelial cells. Accordingly, the first part of the paper provides information about the chemical composition of lipid droplets in the liver of mice fed with a high fat diet (HFD), containing 60 kcal% of saturated fat.¹⁵ In the second part, the formation of LDs in endothelial cells in response to the uptake of arachidonic acid (AA) is shown. This essential polyunsaturated fatty acid (20:4, n-6) represents the major precursor of prostanooids and leukotrienes. AA is stored in lipid droplets in the esterified form and is a modulator of inflammation, which is synthesized and/or released by living cells in response to various environmental factors.

As a reference method, histochemical staining was used, which is often limited by insufficient sensitivity and specificity. The usage of vibrational spectroscopy overcomes these limitations, and the mapping techniques enabled detailed information about the distribution of various compounds simultaneously. Application of nonlinear vibrational microscopy applied to lipid biology has been recently discussed in a review article.¹⁶ Here, we show that linear confocal Raman microscopy, which is becoming a popular and accessible technique, offers detailed chemical information on LDs including depth profiling and thus can be applied to generate high spatial resolution 3D images.¹⁷

MATERIALS AND METHODS

To study lipid droplets in tissue, an experimental dietary model of liver steatosis was used. 6-week old, male C57BL/6J mice were fed for 15 weeks with a HFD containing 60% of calories from saturated fat (Research Diets, USA). As a control, C57BL/6J mice were fed with an AIN-93G diet (standard control diet for early growth and reproduction). Each group contained 3 animals. After sacrificing the animals, livers were frozen in an optimal cutting temperature (OCT) formulation and cut in a cryostat chamber (Leica CM 1950) at a temperature of -23 °C into 10 μm thick sections. Samples were then placed on CaF₂ slides, fixed with 4% buffered formalin solution for 10 min, and subsequently washed with distilled water (2 × 5 min). In both cases (HFD and AIN-93G diet), samples were obtained from three individuals (over a dozen from each).

Primary human aortic endothelial cells (HAoEC) were purchased from Gibco and cultured in supplemented endothelial cell growth medium (EGM-2MV from Lonza). The cell cultures were incubated in a 37 °C, 5% CO₂/95% air, humidified cell culture incubator. Confocal Raman imaging was applied to monitor the molecular composition changes in a single endothelial cell as a result of the uptake of arachidonic acid (AA) from a culture of living human aorta endothelial cells (HAoEC). Cells directly grown onto calcium fluoride windows (CaF₂, 25 × 2 mm, Pike Technologies, U.S.) were exposed to 25 μM sodium salt of arachidonic acid (AANa, Sigma-Aldrich) for 24 h. A second set of cells grown in medium with the addition of sterile water (AANa solvent) served as the control. After 24 h, cells were fixed for 4 min with 4% paraformaldehyde

and stored in isotonic phosphate buffer (PBS, Gibco), pH = 7 at 4 °C until data acquisition.

Raman mapping was performed using a Confocal Raman Imaging system Witec alpha 300 equipped with a 60× water immersion objective (Nikon Fluor, NA = 1) and a 100× air objective (Olympus, MPlan FL N, NA = 0.9) for cells and tissues, respectively. Raman spectra from cells and liver tissue were recorded using a 488 nm solid state laser (laser power of ca. 15 mW at the sample) and a 532 nm Nd:YAG laser (laser power in the range of 6–12 mW), respectively. For liver tissue, the laser power was adjusted individually for each sample to minimize thermal effects.

The scattered light was directed to a spectrometer using a 50 μm core diameter multimode fiber, which also acts as the pinhole for confocal detection. The spectrometer was equipped with a back-illuminated CCD camera and 600 grooves per mm grating (BLZ = 500 nm).

Raman spectroscopic mapping of cells was performed by collecting spectra with 0.5 s exposure time and moving the sample in increments of 0.6 μm (65 × 40 μm², 108 × 66 points). Cell depth profiling was performed by measuring 9 μm (volume of 13 × 28 × 9 μm³), measured as nine layers in a stack for every 1.0 μm in the z-direction from top to bottom. 3D-spectra were collected using 0.4 s exposure time and sampling density of 0.6 μm (13 × 28 × 9 μm³, 21 × 46 points). The total exposure time was ca. 2 h (1 h per Raman map of the entire cell and an additional 1 h for depth profiling of the selected area (7 min per layer)). Spectral measurements of the tissues were performed with an integration time of 0.3–0.5 s and spectral resolution of 3 cm⁻¹. Imaged areas differed in size between samples, covering both: small (approximately 15 × 15 μm², 42 × 42 points) and larger (~50 × 50 μm², 139 × 139 points) regions. From every animal, 6–8 liver sections were prepared, and at least 3 maps from each section were collected.

Spectral characterization of the lipids was achieved by comparing the spectra with reference lipid spectra. Standards of fatty acids were purchased from Sigma-Aldrich (purity ≥99%) and were measured in their natural physical state at room temperature (solid, saturated fatty acids; liquids, unsaturated fatty acids) with the 100× air objective (Olympus MPLAN, NA = 0.90).

As a reference method, fluorescence staining with Nile Red^{18,19} was also used to investigate lipid accumulation in cells. After 24 h of incubation with AANa, cells were washed twice with PBS, fixed with 4% paraformaldehyde for 4 min, BSA-blocked (1% BSA, 30 min), and counterstained with Hoechst 33342 (Life technologies, Carlsbad, USA) and Nile Red (Sigma-Aldrich) for 10 min at RT. An Olympus Scan[®]R automated fluorescence microscope was used to collect the fluorescence images. Images were captured using a DAPI filter for Hoechst 33342 (targeting DNA in the cell nucleus; ultraviolet excitation with blue emission) and FITC filter for Nile Red (green fluorescence of Nile Red is more specific for lipid droplets). Acquisition of the light was 20 and 150 ms for DAPI and FITC fluorescence, respectively.

Histochemical staining with Oil Red O (a standard diazo dye for neutral lipids and triglycerides) was applied to the liver tissue (a “gold standard” of lipid staining). The ORO staining procedure included the following steps: deionized water (3 min), 60% isopropanol alcohol (2 min), Oil Red (30 min), and deionized water (1 min). After the application of these solutions for a certain amount of time, the slides (tissue) were covered with glycerol gel.

All investigations using animals conform with the “Guide for Care and Use of Laboratory Animals” published by the US National Institutes of Health. The experimental procedure used in the present study was approved by the local Animal Research Committee.

For data preprocessing and spectral analysis Witec Project Plus Software, Bruker Optics Software and R Studio²⁰ (based on statistical software R²) supplemented with the “hyperSpec” package²¹ were used. Preprocessing and analysis was performed in R Studio based on in-house developed scripts.^{22,23} Preprocessing included cosmic spike removal, background subtraction, and normalization to the amide I band. Cosmic spike removal and background subtraction (use of polynomial fit, order 2) were performed using Witec Project Plus Software. Two statistical methods were implemented for data analysis: cluster analysis (CA) and principal component analysis (PCA). The aim of cluster analysis is to group analyzed objects (spectra from the map) into clusters, so that objects (spectra) most similar to each other belong to the same cluster.²³ For the CA, Witec Project Plus Software was used, on the basis of k-means clustering, Ward’s algorithm, and Euclidean distance. PCA involves an orthogonal transformation, which aims at converting a set of observations of potentially correlated variables into a set of linear variables or uncorrelated variables (principal components). For PCA, an in-house routine was developed.²³

Iodine values were determined from a prepared calibration curve. For this purpose, Raman spectra were collected for chosen lipid standards, differing in the ratio of C=C/CH₂ (palmitic acid, oleic acid, arachidonic acid). Spectra were then subjected to preprocessing procedures, and the ratios of bands at 1656 to 1444 cm⁻¹ were calculated (on the basis of the area underneath the bands in carefully chosen spectral ranges). The procedure was applied to spectral ranges described elsewhere.²⁴ A calibration curve was prepared on the basis of the literature-given iodine values and determined by taking the ratio of I_{1656}/I_{1444} . The ratios for 395 spectra extracted from lipid droplets in the HFD samples were calculated using this approach. Exactly the same preprocessing steps, as well as ranges of integration, were used for the LDs spectra.

RESULTS AND DISCUSSION

Lipid Droplets (LDs) in Steatotic Liver Section. The aim of this part of the study was to show the utility of Raman

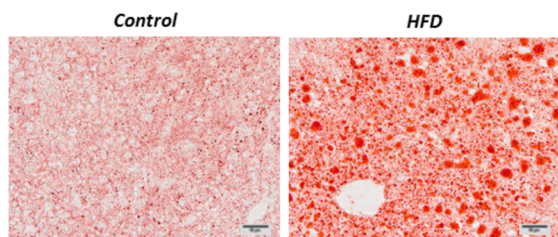


Figure 1. Representative pictures of an Oil Red O stained section of liver taken from mice fed for 15 weeks with a high fat diet (HFD) compared to a control (AIN-93G) diet. Original magnification, 200×. Scale bar = 50 μm.

spectroscopy for obtaining information about chemical composition of lipid droplets formed in liver tissue as a result of pathological changes induced by HFD.¹⁵ As shown in Figure 1, an abnormal accumulation of lipids in the liver in the form of

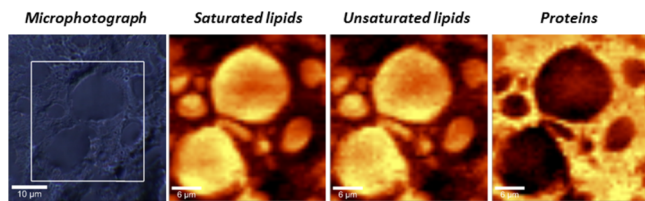


Figure 2. A microphotograph (first on the left) of the mapped area (31.9 μm × 34.0 μm, 87 × 94 points) of the liver tissue section taken from C57BL/6J mice fed a high fat diet (60 kcal% of saturated fat) along with the results of integration analysis (three right-most images, respectively) in ranges: 1420–1480 cm⁻¹ (saturated lipids), 1645–1675 cm⁻¹ (unsaturated lipids), and 1200–1260 cm⁻¹ (amide III, proteins).

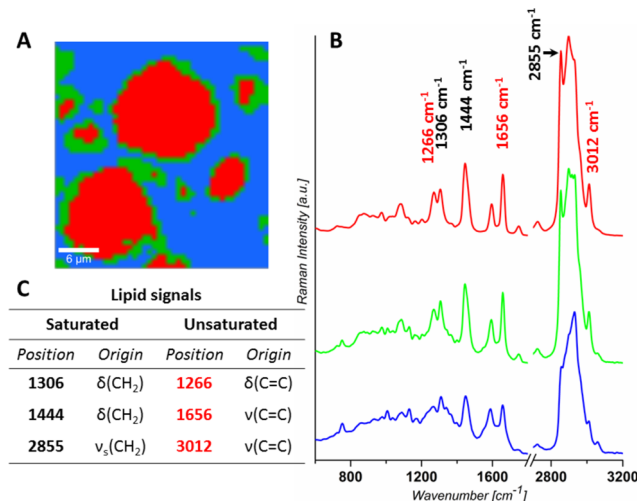


Figure 3. Cluster analysis (k-means) results (A) for the Raman map shown on Figure 6 with the corresponding average spectra (in the ranges: 600–1800 cm⁻¹ and 2800–3200 cm⁻¹) with marked significant lipid bands (B) and the table with their assignments (C).

droplets can be clearly visualized by Oil Red O staining (Figure 1).

Confocal Raman microspectroscopy combined with chemometric analysis was the method of choice to acquire chemical information directly from lipid droplets²⁵ in a nondestructive way.²⁶ Raman mapping enables the investigation of a large sample area, which is important because the lipid droplets can reach tens of μm in diameter. The round shape of the LDs has an influence on the intensity of the spectra collected from the droplet and the surrounding tissue. Moreover, huge variations of intensities of the bands corresponding to lipids can be noticed between droplets of different size. These differences have an impact on the results obtained by the integration of the marker bands. As a consequence, small droplets (~6 μm in diameter) seem to be less visible on the distribution map on the basis of the integration of bands corresponding to lipids (Figure 2). By focusing on a huge droplet (~15 μm in diameter), protruding above the flat surface of the tissue, signals from the surrounding tissue are consequently weakened.

Moreover, the droplet size may have an impact on the spectral profile originating from areas corresponding to small and large droplets. Despite the fact that the sections are fixed and assuming that the tissue surface (after cutting) is flat, the shape of the droplets in deeper sections of tissue remains round. Therefore, a large droplet (with a larger diameter)

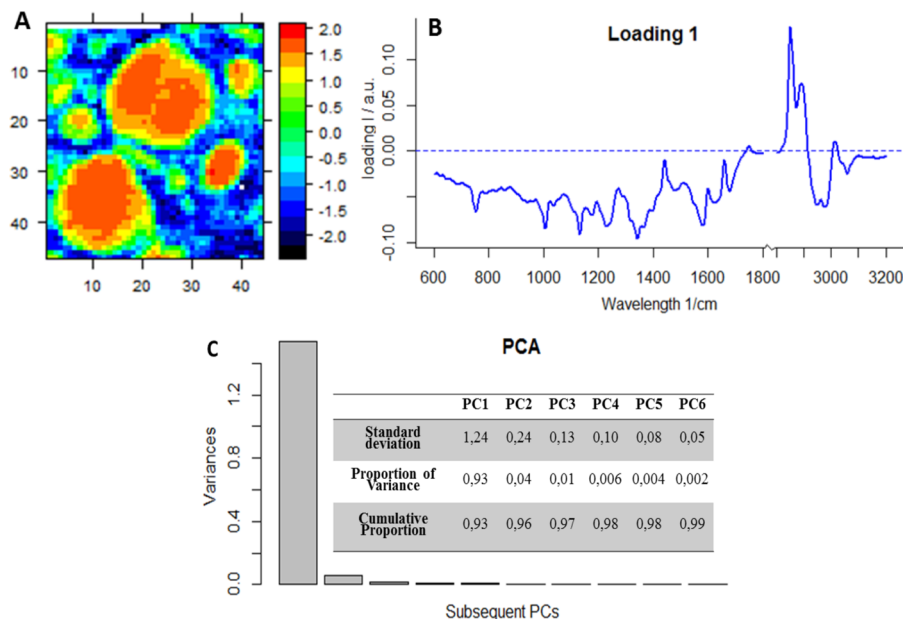


Figure 4. Principal component analysis (PCA) from spectra extracted from the Raman map shown in Figure 3: distribution of score 1 (A), corresponding loadings 1 (in the ranges: 600–1800 cm^{-1} and 2800–3200 cm^{-1}) (B), and a summary of subsequent PCs importance (C).

Table 1. Ratio of Intensities of Selected Bands

mice	I_{1656}/I_{1444}		I_{1266}/I_{1301}		I_{3012}/I_{2855}	
	value	SD ^a	value	SD	value	SD
1	0.69	0.03	0.83	0.05	0.24	0.01
2	0.70	0.04	0.88	0.08	0.28	0.02
3	0.69	0.02	0.79	0.03	0.25	0.01
average	0.69	0.005	0.83	0.04	0.26	0.02

^aStandard deviation calculated for each mouse; SD value for average calculated as deviation between individuals.

corresponds to a larger volume of lipids and occupies a larger area as we enter deeper into the tissue. As a consequence, the larger size of the droplet results in the droplet sinking to greater depth, and therefore, the signal (and thus the spectrum) from this area will have a purely lipidic character with intense lipid bands, whereas the spectrum from the small droplet will contain signals from the droplet and, possibly, a small proportion of signals from the tissue underneath. As the droplet shape is round in deeper compartments of the tissue, the profile of the spectrum will change when approaching the droplet boundary.

To minimize the problem of fluctuating lipid signals caused by varying degrees of laser focus, cluster analysis was applied (Figure 3). Since the differences in the spectral profile of LDs and the surrounding tissue are significant, the large droplets are grouped together with the smaller ones into the red class (Figure 3A). The “intermediate” class (marked as green in Figure 3C) was selected at the border of the droplets where both signals of lipids and tissue are observed. Lipid signals decrease, while bands from other chromophores are increased, e.g., the bands at 755 and 1134 cm^{-1} originate from heme. The distribution of saturated versus unsaturated lipids in liver LDs is homogeneous. It is confirmed by the distribution maps (Figure 2). Further clustering of the lipid class reveals only the differences between the overall intensity of spectra, due to a

different focus on different parts of the sample. The ratio of intensity of saturated vs unsaturated bands remains constant.

The changes can also be noticed in the high wavenumber range (2800–3200 cm^{-1}). In the lipid-class spectrum (Figure 3B, red), the dominant bands in this region are seen at 2855 cm^{-1} (CH_2 symmetric stretch of lipids), 2896 cm^{-1} (CH_2 asymmetric stretch of lipids), and 3012 cm^{-1} (stretching vibrations of $\text{C}=\text{C}$ in unsaturated lipids). For the tissue class (Figure 3B, blue), the most intense signal occurs at 2933 cm^{-1} corresponding to the CH_2 stretching vibration of proteins.

The composition of lipid droplets as well as the changes in the spectral profile associated with the droplet borders can be visualized in detail with PCA. Figure 4C shows that the first principal component explains 93% of differences between spectra within the map. The differences in the range of 2800–3200 cm^{-1} , particularly the presence of bands at 2855 and 3012 cm^{-1} , appear to be the most important factor influencing the distribution (Figure 4B). Positive values on the distribution map for score 1 (Figure 4A) correspond to the distinct presence of these bands. The second significant feature differentiating the spectra appears to be the presence of resonantly enhanced heme bands (i.e., at 755, 1134, and 1592 cm^{-1}) accompanied by other bands attributed to proteins (e.g., at 1005 and 1239 cm^{-1}). For loading 1, the presence of lipid signals is correlated with an absence of protein (and other components). The distribution map of score 1 indicates the highest values in the central part of the droplet. Because the composition of the tissue includes both contributions from the lipid droplets and the surrounding tissue, PCA was also performed on different regions within the map, corresponding to LDs only. No specific distribution of lipids within the droplet was found, as they tend to be homogeneous in their composition (results presented in Supporting Information).

Chemometric tools are excellent for identifying areas of lipid droplets, which is particularly important when small droplets ($\sim 6 \mu\text{m}$ in diameter or less) are studied. Therefore, the Raman approach can be used either for research at an early stage of LDs formation or to study of the effectiveness of potential

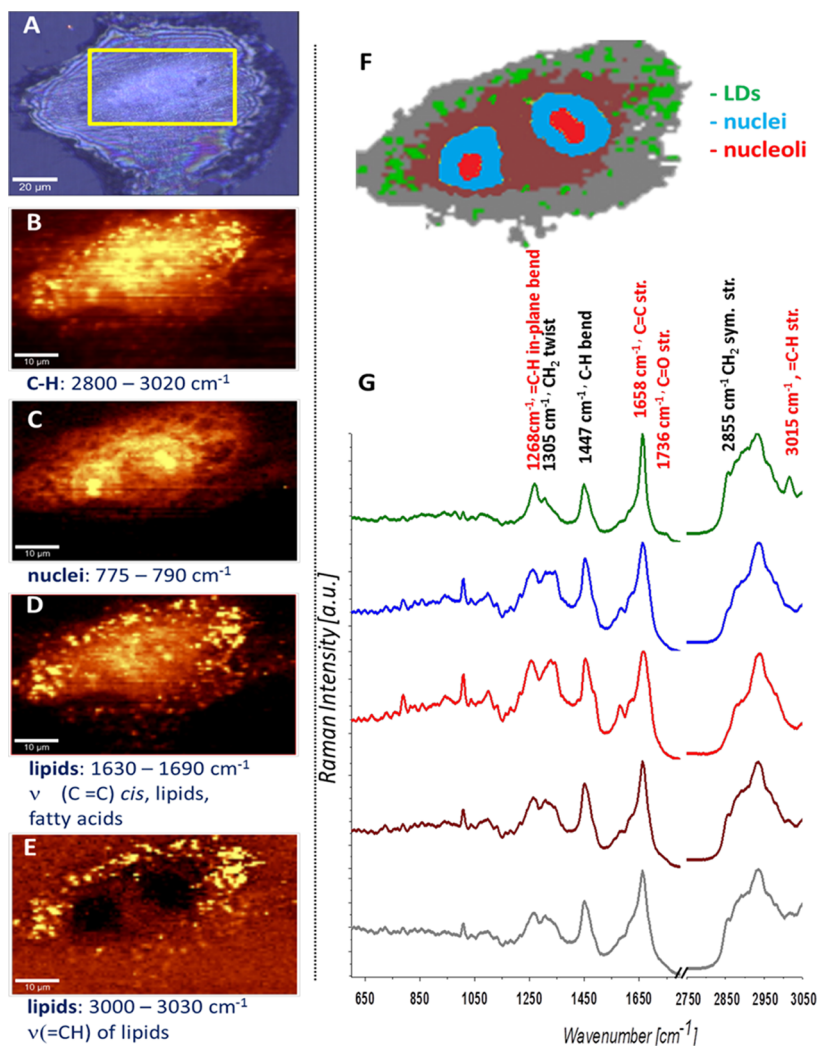


Figure 5. Left panel (A–E): a microphotograph of the HAOEC cell mapped area ($65 \times 40 \mu\text{m}^2$, 108 \times 66 points) and integration maps over the $2800\text{--}3020\text{ cm}^{-1}$, $775\text{--}790\text{ cm}^{-1}$, $1630\text{--}1690\text{ cm}^{-1}$, and $3000\text{--}3030\text{ cm}^{-1}$ ranges, respectively. Right panel (F, G): Cluster map from an HAOEC cell (F) obtained by the application of k-means (5 clusters: blue class, nuclei; red class, nucleoli; brown class, cytoplasm with small organelles, e.g., mitochondria, endoplasmic reticulum; green class, lipid droplets (LDs); gray class, mostly subcortical cytoplasm and membrane) with the average spectra of clusters (G). Raman intensity from the bands in the region of $600\text{--}1800\text{ cm}^{-1}$ is enhanced 3–3.5 times relative to signals in the $2800\text{--}3200\text{ cm}^{-1}$ range to emphasize their spectral differences.

drugs. Raman spectroscopy also enables the determination of the degree of lipid unsaturation.^{25,27–32} Several lipid bands were selected, and their ratios were calculated (Table 1). It is important to take a large number of spectra from the biological material and ensure that there are adequate numbers of individual mice included in the study. The second important aspect is to use exactly the same procedure for data preprocessing. Finally, to compare the data, it is necessary to apply the same integration regions for the bands of interest.

Three ratios were selected as a potential criterion for lipid unsaturation: I_{1656}/I_{1444} , I_{1266}/I_{1301} , and I_{3012}/I_{2855} . The largest variation both within single individuals (0.03–0.08) as well as among them (0.04) is observed in the case of the I_{1266}/I_{1301} ratio. Additionally, this value appears to be useful only in the case of spectra with a very distinct lipid profile, as the location of these bands can be obscured by the presence of heme. Spectra with a sufficiently distinct lipid profile were obtained only from large lipid droplets ($\sim 15 \mu\text{m}$ in diameter or more), which makes it significantly difficult to use this approach for the small droplets (e.g., to monitor their development at early

stages of formation). On the other hand, the criterion based on the high wavenumber range (I_{3012}/I_{2855}) exhibits the least deviation within the same individual (0.01–0.02) and a relatively small deviation among them (0.02). However, it should be noted that the band at 2855 cm^{-1} is considerably larger than the band at 3012 cm^{-1} . Therefore, even a large increase in the area under the band at 3012 cm^{-1} will cause only a small change of the value of I_{3012}/I_{2855} . Thus, although these bands are clear markers of lipid droplets, their ratio cannot be a sensitive indicator for changes in the degree of unsaturation. The most useful, in terms of application to the analysis of droplets for a wide range of sizes and with the highest sensitivity to the changes, proved to be the ratio of the bands at 1656 to 1444 cm^{-1} . This ratio was found to be very reliable between individuals (SD: 0.005), while variation within a single individual (0.02–0.04) is acceptable. However, the overlapping of the band arising from lipids C=C stretch with the amide I mode must also be taken into account. As this problem has already been widely discussed elsewhere,²⁴ here, we only emphasize the fact that the protein content in the

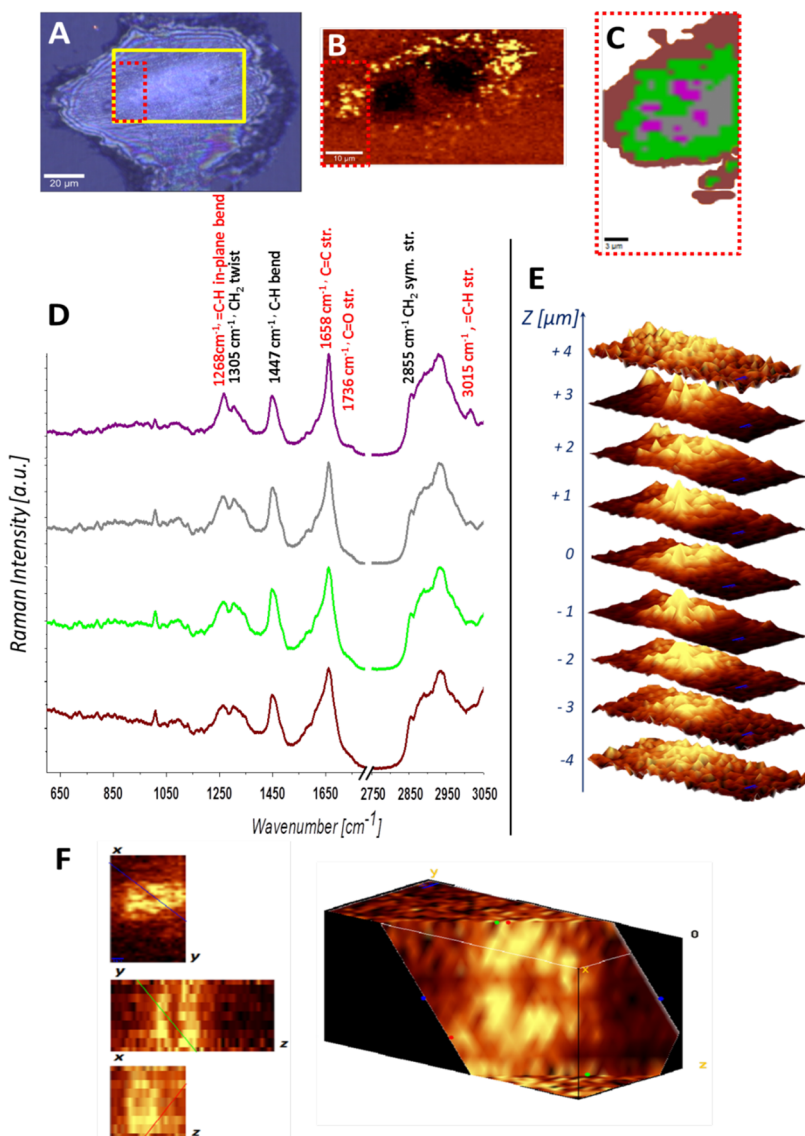


Figure 6. Confocal Raman imaging of HAoEC cell with LDs. (A) A micrograph of the cell with marked area measured in B (yellow square) and in C–F (red dotted square), (B) integration map over the $3000\text{--}3030\text{ cm}^{-1}$ range, (C) cluster map of the fifth layer ($0\text{ }\mu\text{m}$), obtained by application of k-means (4 clusters: violet, LDs; gray and green, cytoplasm with small organelles; brown, mostly subcortical cytoplasm and membrane) with the average spectra of clusters (D), (E) an imaging-stack of LDs covering $13 \times 28 \times 9\text{ }\mu\text{m}^3$ of the cell (integration maps over $1630\text{--}1690\text{ cm}^{-1}$), (F) a cross-section of the reconstructed 3D image. Raman intensity of the bands in the fingerprint region ($600\text{--}1800\text{ cm}^{-1}$) is enhanced 3–3.5 times relative to signals in the $2800\text{--}3200\text{ cm}^{-1}$ range to emphasize their spectral differences.

droplets is negligible and hence will not affect the result significantly. Moreover, the application of the same preprocessing and ranges for band integration will improve the quality of the obtained results. The method can be used to determine the degree of lipid unsaturation based on the number of single bonds $n(\text{C}=\text{C})/n(\text{CH}_2)$ directly from the calibration curve based on the iodine value. For liver tissue from mice fed with HFD for 15 weeks, the iodine value was calculated as 96 ± 6 (calibration data not shown), which indicates a relatively high amount of saturated lipid in the droplets. For comparison, the iodine value for livers obtained from mice fed for 15 weeks on a control diet was 127 ± 8 .

Lipid Droplets (LDs) in Endothelial Cells. In this study, confocal Raman high resolution imaging was used to monitor the formation of lipid droplets in single endothelial cells in culture cultured with arachidonic acid. LDs as well as unsaturated fatty acids can be easily identified in Raman

spectra by bands at 1660 and $\sim 3015\text{ cm}^{-1}$ due to the stretching mode of $=\text{C}-\text{H}$ associated with $\text{C}=\text{C}$ double bonds. The intensity of the 3015 cm^{-1} mode is approximately proportional to the number of $\text{C}=\text{C}$ double bonds in the lipid molecule. Spectra presented in Figure 5 were scaled to the maximum intensity of the amide I band and the C–H stretching mode in the high wavenumber range. The scaling factor for the intensity of bands in the high spectral range ($2800\text{--}3020\text{ cm}^{-1}$) is approximately 3–3.5 and was used to emphasize their spectral differences.

Figure 5 presents two-dimensional spectral maps and chemical images calculated by integrating: the intensity of the C–H stretching vibrations of aliphatic molecules in the $2800\text{--}3020\text{ cm}^{-1}$ range (Figure 5B), cytosine ring vibration of DNA in the $775\text{--}790\text{ cm}^{-1}$ range (Figure 5C), *cis* $\text{C}=\text{C}$ stretching vibration at the 1658 cm^{-1} range (Figure 5D), and stretching vibrations of the $=\text{C}-\text{H}$ bond associated with $\text{C}=\text{C}$ double

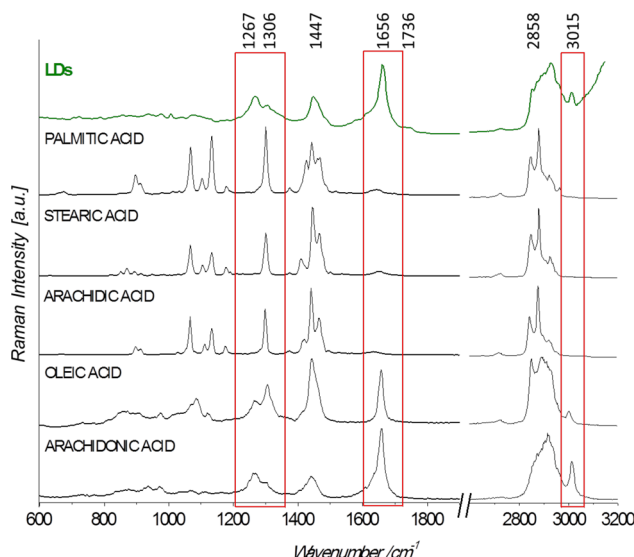


Figure 7. Comparison of average spectrum of endothelial LDs with Raman spectra of selected saturated and unsaturated fatty acids.

bonds (Figure 5E). Bright and dark regions in Figure 5B–E are related to differences in the content and density of biochemical components in proteins and lipids (Figure 5B). Integrated intensities of Raman bands in the 2800–3020 cm^{-1} region reflect the differences in thickness, density, and volume of the measured sample. The highest signal is observed for LDs and the nucleoli in the nucleus.

Figure 5F,G shows the result of k-means cluster analysis (KMCA) in the 600–1800 cm^{-1} range. KMCA was carried out for preprocessed and normalized spectra by using the Manhattan distance. KMCA results were obtained using WITec Project Plus software. The chemical image enables observation of LDs and their distribution in the cytoplasm. Additionally, the main subcellular structures can be selected and observed individually (e.g., nucleus, nucleolus, cytoplasm,

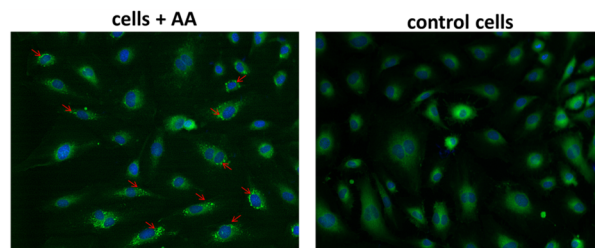


Figure 9. Lipid droplets in cells, visualized using Nile Red neutral lipid stain (green color, FITC): left, cells exposed on AA for 24 h; right, control cells. Blue color (DAPI) corresponds to cell nuclei stained using Hoechst.

and the cell membrane). All five clusters are color coded (Figure 5F), and for each cluster, the average spectrum is shown (Figure 5G).

Additionally, in order to obtain multidimensional information about distribution and size of LDs, confocal Raman microimaging was used as a noninvasive tool to illustrate 3D distribution of lipid droplets in the single endothelial cell. For a small area of a cell rich in LDs (Figure 6E,F), the depth profiling in the volume of $13 \times 28 \times 9 \mu\text{m}^3$, measured as nine layers in a stack for every 1.0 μm in the z-direction up to down, was carried out. A well established protocol for 3D Raman imaging¹⁷ was applied in this study to enable a detailed investigation of the shape and size of cytoplasmic LDs. Confocal measurements confirmed that endothelial lipidic structures observed as a result of AA uptake are localized inside the cell. The virtual reconstructed 3-dimensional image of the cell fragment rich in LDs (Figure 6F) is presented as a volume within a xyz-coordination system. The reconstructed 3D image is presented in Figure 6F as a volume within an xyz-coordination system. By using the volume viewer option and rendering with an intersection in the xy-, zy-, and xz-plane, it was possible to obtain a 3D cross-section of the cell together with selected subcellular structures. For the fifth layer (at the

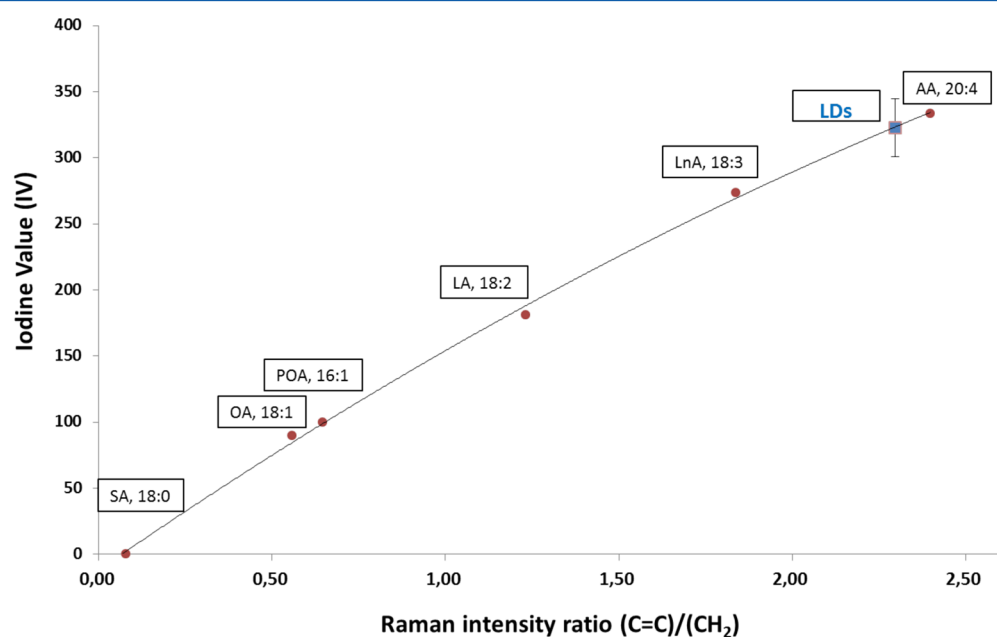


Figure 8. A calibration curve for selected standards of fatty acids (differing in the degree of unsaturation), which correlates iodine value (degree of unsaturation) with their Raman intensity ratio of $(\text{C}=\text{C})/(\text{CH}_2)$ modes ($1656/1444 \text{ cm}^{-1}$).

level of $0\text{ }\mu\text{m}$), the KMCA analysis with four clusters was performed (Figure 6C,D). An average spectrum corresponding to the violet cluster shows a characteristic profile, and the observed Raman bands indicate the presence of organelles in the cytoplasm rich in unsaturated lipids. The size, shape, distribution, and biochemical composition of the observed structures confirmed that they are lipid droplets.

Average spectra from LDs were compared with the spectra of selected saturated and unsaturated fatty acids (Figure 7) in order to determine the biochemical composition of the lipid droplets (LDs). The Raman bands at 1267, 1305, 1447, 1656, 1736, 2858, and 3015 cm^{-1} dominate the spectral profile of LDs and are assigned to polyunsaturated fatty acids (PUFA). Analysis of LDs averaged spectrum compared to the unsaturated fatty acid spectrum indicates that the main component of LDs in endothelial cells treated with arachidonic acid is arachidonic acid taken up by the cells.

Spectroscopic measurements also enable determination of the degree of unsaturation directly in the lipid droplets. For that purpose, two marker bands: at 1656 cm^{-1} (originating from C=C stretching mode of unsaturated lipids) and 1444 cm^{-1} (corresponding to CH₂ bending mode of saturated lipids) were used. By constructing a calibration curve for chosen standards of fatty acids (differing in the degree of unsaturation),²⁸ it was possible to predict the degree of unsaturation of the lipids measured directly in the LDs (Figure 8).

As a complementary method for LDs identification, the fluorescence microscopy was applied. Endothelial cells after a 24 h incubation with $25\text{ }\mu\text{M AA}$ were stained using neutral lipid dye (Nile Red) and observed with the imaging cytometry. Fluorescence measurements using Nile Red confirmed the Raman results that the endothelial cells stimulated by AA can form lipid droplets inside the cytoplasm (Figure 9). An increased number of lipid droplets is observed in human aorta endothelial cells (HAoEC) exposed to $25\text{ }\mu\text{M}$ of arachidonic acid for 24 h.

CONCLUSIONS

In this work, we demonstrate that high resolution Raman mapping can be successfully applied to study the formation of lipid droplets at the cellular level. Lipid droplets were identified on the basis of their chemical composition; additionally, their size and distribution was visualized in 3-dimensions. We characterized the lipid droplets in hepatocytes in steatotic liver as well as in endothelium treated with exogenous arachidonic acid. The Raman-based approach was useful to get a better understanding of the role LDs play in health and diseases, in particular in the endothelium, which has not been previously studied in this context. The availability of confocal Raman spectrometers and their technical development together with advanced data analysis opens new perspectives for this method to be used to study LDs at subcellular levels in submicrometer scale and in 3D.

ASSOCIATED CONTENT

Supporting Information

Additional information as noted in text. This material is available free of charge via the Internet at <http://pubs.acs.org>.

AUTHOR INFORMATION

Corresponding Author

*E-mail: baranska@chemia.uj.edu.pl

Notes

The authors declare no competing financial interest.

ACKNOWLEDGMENTS

The project was supported by National Science Center (DEC-2013/08/A/ST4/00308) and by the European Union under the European Regional Development Fund (grant coordinated by JCET-UJ, POIG.01.01.02-00-069/09). K.M. acknowledges the support from the project Interdisciplinary PhD Studies "Molecular sciences for medicine" (cofinanced by the European Social Fund within the Human Capital Operational Programme). K.M. and K.K. acknowledge the Marian Smoluchowski Krakow Research Consortium "Matter Energy Future" for the granted scholarships (the KNOW status for the 2012–2017 by the Ministry of Science and Higher Education). Associate Professor Bayden R. Wood proofread the manuscript.

REFERENCES

- (1) Reue, K. *J. Lipid Res.* **2011**, *52*, 1865–1868.
- (2) Fujimoto, T.; Parton, R. G. *Cold Spring Harbor Perspect. Biol.* **2011**, *3*, a004838.
- (3) Melo, R. C. N.; D'Avila, H.; Wan, H.-C.; Bozza, P. T.; Dvorak, A. M.; Weller, P. F. *J. Histochem. Cytochem.* **2011**, *59*, S40–S56.
- (4) Walther, T. C.; Farese, R. V., Jr. *Biochim. Biophys. Acta* **2009**, *1791*, 459–466.
- (5) Murphy, D. J. *Prog. Lipid Res.* **2001**, *40*, 325–438.
- (6) Martin, S.; Parton, R. G. *Nat. Rev. Mol. Cell Biol.* **2006**, *7*, 373–378.
- (7) Kuerschner, L.; Moessinger, C.; Thiele, C. *Traffic* **2008**, *9*, 338–352.
- (8) Murphy, S.; Martin, S.; Parton, R. G. *Biochim. Biophys. Acta* **2009**, *1791*, 441–447.
- (9) Kohlwein, S. D.; Veenhuis, M.; van der Klei, I. J. *Genetics* **2013**, *193*, 1–50.
- (10) Bozza, P. T.; Magalhães, K. G.; Weller, P. F. *Biochim. Biophys. Acta* **2009**, *1791*, S40–S51.
- (11) Bozza, P. T.; Magalhães, K. G.; Weller, P. F. *Biochim. Biophys. Acta* **2009**, *1791*, 540–551.
- (12) Thiele, C.; Spandl, J. *Curr. Opin. Cell Biol.* **2008**, *20*, 378–385.
- (13) Ohsaki, Y.; Cheng, J.; Suzuki, M.; Shinohara, Y.; Fujita, A.; Fujimoto, T. *Biochim. Biophys. Acta* **2009**, *1791*, 399–407.
- (14) Melo, R. C. N.; Paganoti, G. F.; Dvorak, A. M.; Weller, P. F. *PLoS One* **2013**, *8*, No. e59578.
- (15) Takahashi, Y.; Soejima, Y.; Fukusato, T. *World J. Gastroenterol.* **2012**, *18*, 2300–2308.
- (16) Zumbusch, A.; Langbein, W.; Borri, P. *Prog. Lipid Res.* **2013**, *52*, 615–632.
- (17) Majzner, K.; Kaczor, A.; Kachamakova-Trojanowska, N.; Fedorowicz, A.; Chłopicki, S.; Baranska, M. *Analyst* **2013**, *138*, 603–610.
- (18) Suzuki, M.; Shinohara, Y.; Fujimoto, T. Histochemical Detection of Lipid Droplets in Cultured Cells. In Taatjes, D.J.; Roth, J., Eds.; *Cell Imaging Techniques Methods and Protocols*; Springer: New York, 2006: pp 483–491.
- (19) Listenberger, L. L.; Brown, D. A. *Curr. Protoc. Cell Biol.* **2007**, *35*, 24.2.1–24.2.11.
- (20) RStudio: *Integrated Development Environment for R* (version 0.96.122); RStudio: Boston, MA, 2012.
- (21) Beleites, C.; Beleites, M. Package "hyperSpec": A package to handle hyperspectral data sets in R; 2012.
- (22) Beleites, C.; Kraft, C.; Popp, J.; Sergo, V. *Gliomas* **2011**, *2*.
- (23) Banas, K.; Banas, A. M.; Gajda, M.; Kwiatek, W. M.; Pawlicki, B.; Breese, M. B. H. *Radiat. Phys. Chem.* **2013**, *93*, 82–86.
- (24) Kochan, K.; Maslak, E.; Kostogrys, R.; Chłopicki, S.; Baranska, M. *Biomed. Spectrosc. Imaging* **2013**, *2*, 331–337.

- (25) Kochan, K.; Marzec, K. M.; Chruszcz-Lipska, K.; Jasztal, A.; Maslak, E.; Musiolik, H.; Chłopicki, S.; Baranska, M. *Analyst* **2013**, *38*, 3885–3890.
- (26) Krafft, C.; Dietzek, B.; Popp, J. *Analyst* **2009**, *134*, 1046–1057.
- (27) Schulz, H.; Baranska, M. *Vib. Spectrosc.* **2007**, *43*, 13–25.
- (28) Samek, O.; Jonáš, A.; Pilát, Z.; Zemánek, P.; Nedbal, L.; Tříška, J.; Kotas, P.; Trtílek, M. *Sensors* **2010**, *10*, 8635–8651.
- (29) Barthus, R. C.; Poppi, R. J. *Vib. Spectrosc.* **2001**, *26*, 99–105.
- (30) Afsetha, N. K.; Wold, J. P.; Segtnana, V. H. *Anal. Chim. Acta* **2006**, *572*, 85–92.
- (31) Olsen, E. F.; Rukke, E.-O.; Flåtten, A.; Isaksson, T. *Meat Sci.* **2007**, *76*, 628–634.
- (32) Afseth, N. K.; Wold, J. P.; Segtnan, V. H. *Anal. Chim. Acta* **2006**, *572*, 85–92.